Collagen and elastin cross-linking is altered during aberrant late lung development associated with hyperoxia

Ivana Mižíková,[1] Jordi Ruiz-Camp,[1] Heiko Steenbock,[3] Alicia Madurga,[1,2] István Vadász,[2] Susanne Herold,[2] Konstantin Mayer,[2] Werner Seeger,[1,2] Jürgen Brinckmann,[3,4] and Rory E. Morty[1,2]

[1]*Department of Lung Development and Remodelling, Max Planck Institute for Heart and Lung Research, Bad Nauheim, Germany;* [2]*Department of Internal Medicine (Pulmonology), University of Giessen and Marburg Lung Center, German Center for Lung Research, Giessen, Germany;* [3]*Institute of Virology and Cell Biology, University of Lübeck, Lübeck, Germany; and* [4]*Department of Dermatology, University of Lübeck, Lübeck, Germany*

Mižíková I, Ruiz-Camp J, Steenbock H, Madurga A, Vadász I, Herold S, Mayer K, Seeger W, Brinckmann J, Morty RE. Collagen and elastin cross-linking is altered during aberrant late lung development associated with hyperoxia. *Am J Physiol Lung Cell Mol Physiol* 308: L1145–L1158, 2015. First published April 3, 2015; doi:10.1152/ajplung.00039.2015.—Maturation of the lung extracellular matrix (ECM) plays an important role in the formation of alveolar gas exchange units. A key step in ECM maturation is cross-linking of collagen and elastin, which imparts stability and functionality to the ECM. During aberrant late lung development in bronchopulmonary dysplasia (BPD) patients and animal models of BPD, alveolarization is blocked, and the function of ECM cross-linking enzymes is deregulated, suggesting that perturbed ECM cross-linking may impact alveolarization. In a hyperoxia (85% O_2)-based mouse model of BPD, blunted alveolarization was accompanied by alterations to lung collagen and elastin levels and cross-linking. Total collagen levels were increased (by 63%). The abundance of dihydroxylysinonorleucine collagen cross-links and the dihydroxylysinonorleucine-to-hydroxylysinonorleucine ratio were increased by 11 and 18%, respectively, suggestive of a profibrotic state. In contrast, insoluble elastin levels and the abundance of the elastin cross-links desmosine and isodesmosine in insoluble elastin were decreased by 35, 30, and 21%, respectively. The lung collagen-to-elastin ratio was threefold increased. Treatment of hyperoxia-exposed newborn mice with the lysyl oxidase inhibitor β-aminopropionitrile partially restored normal collagen levels, normalized the dihydroxylysinonorleucine-to-hydroxylysinonorleucine ratio, partially normalized desmosine and isodesmosine cross-links in insoluble elastin, and partially restored elastin foci structure in the developing septa. However, β-aminopropionitrile administration concomitant with hyperoxia exposure did not improve alveolarization, evident from unchanged alveolar surface area and alveoli number, and worsened septal thickening (increased by 12%). These data demonstrate that collagen and elastin cross-linking are perturbed during the arrested alveolarization of developing mouse lungs exposed to hyperoxia.

lung development; elastin; collagen; lysyl oxidase; alveolarization

POSTNATAL LUNG DEVELOPMENT in mice is characterized by a period of intensive growth and remodeling of the lung parenchyma, which rapidly (over a period of days) generates a large number of small alveoli and thus maximizes the alveolar surface area over which gas exchange can take place. Secondary septation, the generation of new septa from preexisting septa, which then divide the air spaces, peaks in mice between 4 and 7 days after birth and is largely complete 21 days after birth. In humans, secondary septation is already well underway during late stages of pregnancy, and thus occurs in utero, and continues several years into postnatal life. Disturbances to the formation of secondary septa, such as the arrested secondary septation associated with bronchopulmonary dysplasia (BPD) in humans, leads to malformed lungs with fewer and larger alveoli. This common complication of premature birth is associated with significant morbidity and mortality.

The molecular mechanisms underlying the generation of secondary septa remain poorly understood, but most likely rely on the coordinated action of transcription factors, growth factor signaling, extracellular matrix (ECM) deposition and remodeling, and physical forces, such as breathing motions (41, 42). The generation and shaping of the lung ECM has received much attention in the context of normal and aberrant lung alveolarization (20, 38, 45). Infants with BPD exhibit increased collagen abundance in the lung (14), and collagen fibers and the lung collagen scaffold are malformed (60). There is also evidence of altered elastin turnover, as assessed by urinary excretion of the desmosine elastin cross-link, in infants with BPD (12). These data point to disturbances to ECM production and processing in BPD, which may be mimicked in animal models, employing either hyperoxia, caloric restriction, mechanical ventilation, or preterm delivery as an injurious stimulus in rats, mice, lambs, and baboons (6, 13, 49, 66). The lung histopathology that results is reminiscent of that of BPD in humans, with evident air space enlargement, septal wall thickening, and a reduced number of alveoli, as well as perturbations to ECM structures. Increased collagen levels have been reported in the lungs of hyperoxia-exposed adult rats (44). Elastin has received more attention, since normal elastin production and deposition are critical for proper development of alveoli (43, 57, 58). In hyperoxia-exposed or calorie-restricted mice, late lung development is impeded, and elastic fibers are described to be "irregularly distributed, tortuous, and abruptly terminating" (11). Similarly, in mechanically ventilated preterm lambs, late lung development is also impeded, and excessive production of elastin and accumulation of short, brush-like elastin fibers in the developing lung has been noted (2, 52).

To date, the underlying reasons for these perturbations to ECM structures have remained elusive. Excessive elastase activity has been considered as a mediator of pathological elastin degradation, which might underlie the paucity of elastin and bizarre elastin fiber patterns seen in affected lungs (21–23, 36). Additionally, the altered expression of proteins required for proper elastin fiber assembly has also been suggested to

Address for reprint requests and other correspondence: R. E. Morty, Dept. of Lung Development and Remodelling, Max Planck Institute for Heart and Lung Research, Parkstrasse 1, D-61231 Bad Nauheim, Germany (e-mail: rory.morty@mpi-bn.mpg.de).

uncouple elastin synthesis and the assembly of elastin fibers (7–9). Several recent studies have revealed that the expression and activity of several ECM maturation systems, including collagen and elastin cross-linking enzymes of the lysyl oxidase (33), lysyl hydroxylase (65), and transglutaminase (64) families, are deregulated in both animal models of BPD and in tissues from BPD patients. These observations suggest that improper ECM cross-linking in the developing lung may contribute to disturbed alveolarization. This idea is supported by a recent report that lysyl oxidases play a causal role in the remodeling of the pulmonary vasculature that is associated with pulmonary arterial hypertension (48). Thus it was hypothesized and tested in this study that collagen and elastin cross-linking is perturbed during the arrested alveolarization that is associated with the exposure of mouse neonates to a hyperoxic environment. Additionally, a causal role for lysyl oxidases in generating perturbed ECM cross-linking was explored.

MATERIAL AND METHODS

Animal studies. All animal procedures were approved by the local authorities, the Regierungspräsidium Darmstadt (approvals B2/329 for pilot and P9.5 studies, and B2/1029 for P19.5 studies). For studies using the broad-spectrum lysyl oxidase inhibitor, β-aminopropionitrile (BAPN; A3134, Sigma, St. Louis, MO), a pilot study was first performed with a dose of 15 and 150 mg·kg^{-1}·day^{-1} (three animals per group, observed for 5 days) to assess BAPN tolerance. The upper limit of this dose was based on previous studies with BAPN in adult mice (48). After the pilot study, BAPN was then applied at 15 mg·kg^{-1}·day^{-1} in a well-characterized animal model of BPD, where an arrest of alveolarization can be induced by exposure of newborn mouse pups to normobaric hyperoxia (85% O_2), from the first day of birth, exactly as described previously (4, 33). The normoxia (21% O_2) and the hyperoxia (85% O_2) groups were both further subdivided into two groups, treated with daily intraperitoneal injections of either PBS (serving as solvent vehicle control) or BAPN in PBS (15 mg·kg^{-1}·day^{-1}) for either 9 days [postnatal day (P) 9.5] or 19 days (P19.5). To minimize oxygen toxicity and to avoid potential confounders of milk production caused by changes in inspired oxygen levels, nursing dams were rotated every 24 h between normoxia and hyperoxia. Dams and pups received food ad libitum and were maintained on 12:12-h light-dark cycle.

Gene and protein expression analysis. Real-time reverse transcription-polymerase chain reaction (RT-PCR) and immunoblotting were performed as described previously (3–5, 33, 39, 48, 64, 65). Mouse lung tissue was processed for mRNA isolation and protein isolation essentially as described previously (3, 46). Total RNA was isolated from mouse lung tissue using a peqGOLD Total RNA kit (PEQLAB,

Erlangen, Germany). For immunoblotting, lung tissue was homogenized in a Precellys 24-Dual homogenizer (PEQLAB) in 20 mM Tris-Cl, 150 mM NaCl, 1 mM EDTA, 1 mM EGTA, 1% (vol/vol) NP-40, 1 mM sodium orthovanadate and 1× Complete protease inhibitor cocktail (11836145001; Roche, Mannheim, Germany). Protein concentration was determined by Bradford assay. For real-time RT-PCR analysis, ΔC_t values were calculated as mean C_t (reference gene) − mean C_t (gene of interest), where the *polr2a* mRNA abundance always served as reference. The primers employed for real-time RT-PCR are listed in Table 1. The antibodies used for immunoblot analysis were as follows: rabbit anti-LOX (ab31238; Abcam, Cambridge, UK; 1:500), rabbit anti-LOXL1 (ab81488; Abcam; 1:750), rabbit anti-LOXL2 (ab113960; Abcam; 1:750), rabbit anti-LOXL3 (ab122263; Abcam; 1:250), and rabbit anti-LOXL4 (ab130646; Abcam; 1:100). Loading equivalence was determined using rabbit anti-β-actin (4967; Cell Signaling Technology, Danvers, MA; 1:1,000). All antibodies employed were raised in rabbits and, therefore, the antigen-primary antibody complexes were detected with a goat anti-rabbit IgG conjugated to horseradish peroxidase (31460; ThermoScientific, Rockford, IL; 1:3,000).

Lysyl oxidase activity assay. Lysyl oxidase activity in whole-lung homogenates was assessed essentially as described previously (33), using an Amplex Red-coupled assay marketed as a Lysyl Oxidase Activity Assay kit (ab112139; Abcam). Activity was assessed in freshly isolated total protein samples (10 μg) from whole mouse lung homogenates. Lysyl oxidase activity is reported as the BAPN-sensitive fraction, where the rate of product generation in the linear range over a 20-min period was determined in the presence of 500 μM BAPN subtracted from that obtained from a paired sample in the absence of BAPN. Fluorescence was measured during the exponential phase of enzymatic reaction using Infinite 200 PRO multimode reader (TECAN, Männedorf, Switzerland).

Assessment of collagen and elastin protein and cross-links. Total collagen and elastin levels, as well as the abundance of the collagen cross-links dihydroxylysinonorleucine (DHLNL), hydroxylysylpyridinoline (HP), and hydroxylysinonorleucine (HLNL), and the elastin cross-links desmosine and isodesmosine were determined exactly as described previously for adult mouse lungs and human tissues (10, 48). The nomenclature used in this study refers to the reduced variants of the intermediate collagen cross-links (DHLNL, HLNL). The deposition of elastin and elastin fiber structures was visualized in paraffin-embedded mouse lungs that had been instillation-fixed via a tracheal cannula at a hydrostatic pressure of 20 cmH$_2$O with 4% (wt/vol) paraformaldehyde in PBS for 24 h at 4°C. The lung tissue sections (3 μm) were stained with Hart's elastin stain, as described previously (33).

Design-based stereology. All methods employed in this study for the analysis of lung structure were based on recently published American Thoracic Society/European Respiratory Society recommendations for quantitative assessment of lung structure (25). The proto-

Table 1. *Primers employed for a real-time RT-PCR analysis*

Gene	Primer	Primer Sequence, 5'-3'	Length	Amplicon Size, bp	T_m, °C	Location, bp
lox	Forward	CAG CCA CAT AGA TCG CAT GGT	21	133	60.54	579–599
	Reverse	GCC GTA TCC AGG TCG GTT C	19		60.23	711–693
loxl1	Forward	GAG TGC TAT TGC GCT TCC C	19	225	58.98	1675–1693
	Reverse	GGT TGC CGA AGT CAC AGG T	19		60.23	1899–1881
loxl2	Forward	ATT AAC CCC AAC TAT GAA GTG CC	23	130	58.72	2280–2302
	Reverse	CTG TCT CCT CAC TGA AGG CTC	21		59.50	2409–2389
loxl3	Forward	CTA CTG CTG CTA CAC TGT CAG T	22	133	59.77	133–154
	Reverse	GAC CTT CAT AGG GCT TTC TAG GA	23		59.03	265–243
loxl4	Forward	GCC AAC GGA CAG ACC AGA G	19	139	60.37	216–234
	Reverse	CCA GGT CAA GGC TGA CTC AAA	21		60.20	354–334
polr2a	Forward	CTA AGG GGC AGC CAA AGA AAC	21	209	59.45	808–828
	Reverse	CCA TTC AGC ATA CAA CTC TAG GC	23		59.19	1016–994

T_m, mean temperature; bp, base pairs.

col employed for the design-based stereomorphometric analysis of neonatal mouse lungs has been described in the detail previously (39), based on state-of-the-art methodology (47, 51, 56). Briefly, mouse pup lungs were instillation-fixed through a tracheal cannula at a hydrostatic pressure of 20 cmH$_2$O with 1.5% (wt/vol) paraformaldehyde, 1.5% (wt/vol) glutaraldehyde in 150 mM HEPES, pH 7.4, for 24 h at 4°C (31). Lung tissue blocks were then collected according to systematic uniform random sampling for stereological analysis (50, 62). The total volume of the lungs was measured by Cavalieri's principle (61). Lungs were embedded in toto in agar and cut into slices of 2-mm thickness. Lungs were treated with sodium cacodylate, osmium tetroxide, and uranyl acetate and embedded in glycol methacrylate (Technovit 7100, Heareus Kulzer, 64709003). Each tissue block was cut into sections of 2 μm, and every first and third section of a consecutive series of sections was stained with Richardson's stain. All slides were scanned using a NanoZoomer-XR C12000 Digital slide scanner (Hamamatsu). Analyses were made using the Visiopharm NewCast computer-assisted stereology system (VIS 4.5.3). Analyses included the determination of mean linear intercept (MLI), alveolar septal wall thickness, total alveolar septal volume and surface area, as well as alveolar number, as described previously (39). Approximately 60 tissue section were evaluated per animal for all

parameters, except the determination of alveolar number, in which case ~30 sections per animal were evaluated. In each case, 2–3% of each section was analyzed. The coefficient of error (CE), the coefficient of variation (CV), and the squared ratio between both (CE^2/CV^2) were measured for each stereological parameter, and the quotient threshold was set at <0.5 to validate the precision of the measurements.

Statistical analysis. All statistical data presented in graphs are indicated as means ± SD. Data presented in Tables 2–5 are indicated as means ± SE. Differences between groups were compared by determining *P* values by one-way ANOVA with Tukey's post hoc test for all experiments, except for a unpaired Student's *t*-test analysis used for the RT-PCR analysis (Fig. 1). The *P* values < 0.05 were regarded as significant. All statistical analyses were performed with GraphPad Prism 6.0. Statistical outliers were identified by Grubb's test.

RESULTS

Exposure of immature mouse lungs to 85% O$_2$ drives aberrant lysyl oxidase expression. Previous studies on lysyl oxidase expression in the developing mouse lung using semiquantitative RT-PCR have suggested changes in lysyl oxidase expression over the course of postnatal lung maturation in the mouse,
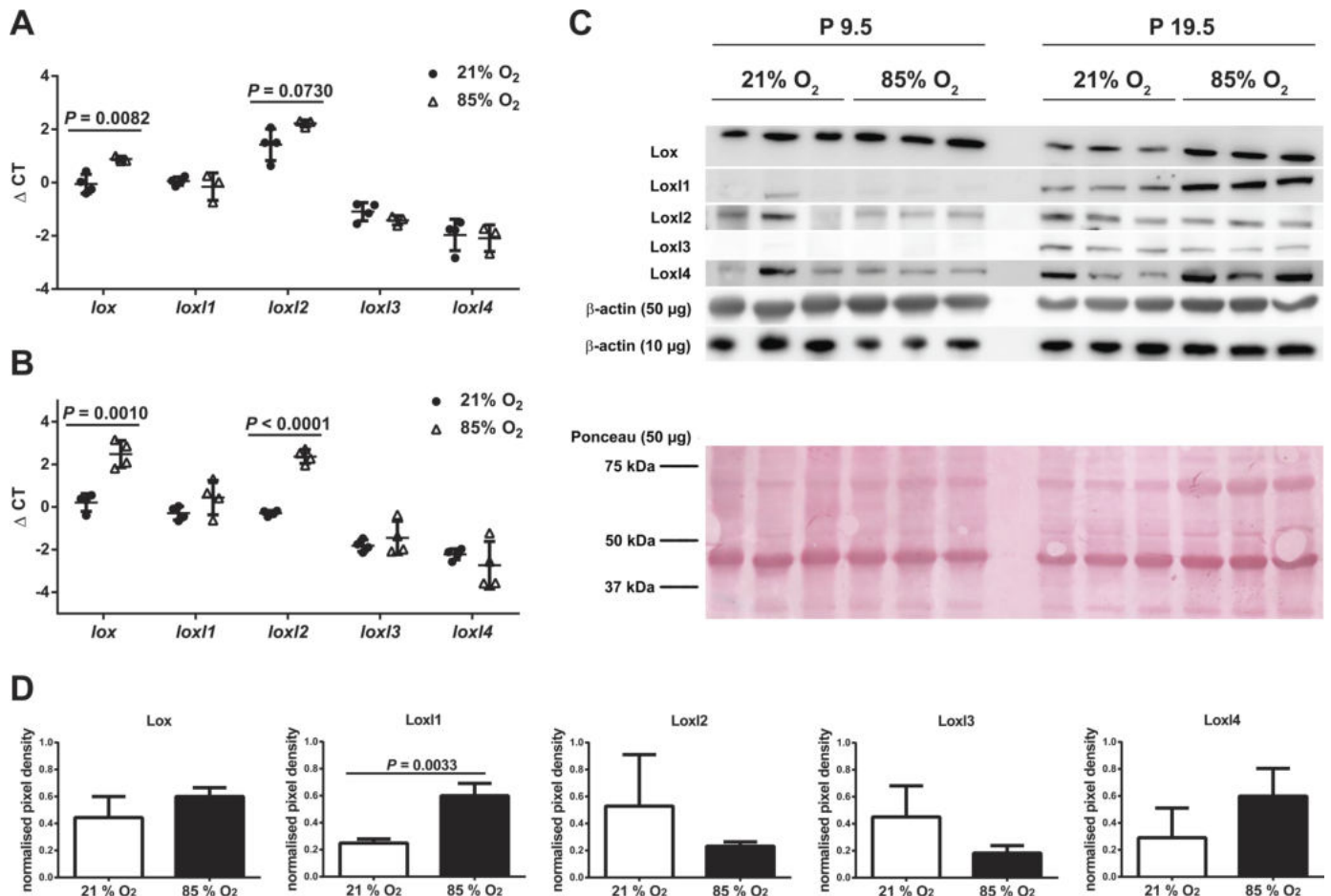

Fig. 1. Lysyl oxidase expression is deregulated during aberrant late lung development. Lysyl oxidase mRNA levels were assessed in lung homogenates from mouse pups exposed to 21% O$_2$ (●) or 85% O$_2$ (△) from the day of birth, at postnatal day (P) 9.5 (*A*) and P19.5 (*B*), by real-time RT-PCR. Values are means ± SD (*n* = 3–5 per group). The *P* values were determined by unpaired Student's *t*-test. *C*: protein expression levels for all five lysyl oxidases were assessed in lung homogenates from mouse pups exposed to 21% O$_2$ or 85% O$_2$ from the day of birth, by immunoblot at P9.5 (*left* side of gel) and P19.5 (*right* side of gel). For lysyl oxidases and the upper β-actin sample, 50 μg of protein were loaded, which yielded overloaded β-actin bands. Hence, a second loading control, in which 10 μg of protein were loaded, is also provided for β-actin. Additionally, the Ponceau S-stained immunoblot membrane is included for the gel run for the 50-μg β-actin immunoblot, to confirm loading equivalence. Three mice per experimental group were evaluated. *D*: densitometric analysis of the data presented in *C* for mice at P19.5, where the pixel densities for lysyl oxidase bands were normalized for the pixel density of the β-actin bands from the same sample. Values are means ± SD. The *P* values were determined by unpaired Student's *t*-test.

Fig. 2. Administration of β-aminopropion-itrile (BAPN) impacted mouse pup viability. A pilot study was conducted where solvent vehicle alone was applied daily (intraperitoneal), or BAPN was applied (intraperitoneal) at dose of 15 or 150 mg·kg^{-1}·day^{-1} (three animals per group, observed for 5 days). *A*: body mass measured at *day 5* for the three groups. Values are means ± SD ($n = 3$ per group). The *P* values were determined by one-way ANOVA with a Tukey's post hoc test. *B*: images of representative mice from each of the three groups. The milk spot is indicated by an arrow, when present. *C*: the experimental protocol applied for subsequent studies. This figure is supported by Supplemental Video S1, in the online supplement.
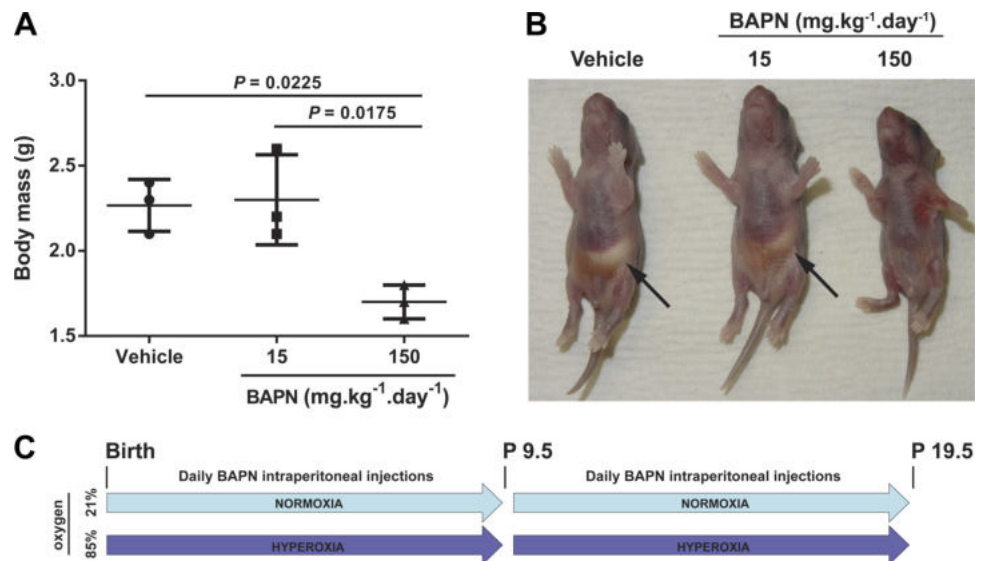
during both normal lung development, as well as arrested late lung development associated with postnatal exposure to hyperoxia (33). Exposure of mouse pups to 85% O$_2$ from birth resulted in persistently upregulated expression of *lox* at both P9.5, by 1.8-fold (Fig. 1*A*), and P19.5, by 5.0-fold (Fig. 1*B*). Additionally, an upregulation in mRNA expression of *loxl2* in response to hyperoxia was also noted at P9.5 (2.1-fold; Fig. 1*A*) and P19.5 (6.6-fold; Fig. 1*B*). While the changes on LoxL2 expression were not evident by immunoblot, the elevated expression of Lox was evident by immunoblot at P9.5 and P19.5 (Fig. 1*C*). Additionally, elevated protein levels of LoxL1 and LoxL4 were evident in the lungs of mouse pups exposed to 85% O$_2$ from the day of birth, at P19.5 (Fig. 1*C*).

Administration of a lysyl oxidase inhibitor can normalize lysyl oxidase activity in the lungs of mice exposed to 85% O$_2$. Administration of the broad-spectrum lysyl oxidase inhibitor BAPN at a dose of 150 mg·kg^{-1}·day^{-1} was toxic to developing mouse pups and results in impaired development evident from reduced body mass of 1.7 ± 0.1 g at P5.5 (Fig. 2*A*), reduced milk intake (note missing milk spot in the mouse pup documented in Fig. 2*B*), and reduced mobility (as evident in Supplemental Video S1; the online version of this article contains supplemental data). In contrast, mice receiving a dose one-log lower, at 15 mg·kg^{-1}·day^{-1}, exhibited normal body mass (Fig. 2*A*), normal milk intake (Fig. 2*B*), and normal mobility (see Supplemental Video S1 in the online supplement). For this reason, BAPN was applied at a dose of 15 mg·kg^{-1}·day^{-1} for further studies, with mouse lungs harvested at P9.5 and P19.5 for analysis (Fig. 2*C*). The dose of 15 mg·kg^{-1}·day^{-1} was sufficient to normalize lysyl oxidase activity in developing lungs from mice exposed to 85% O$_2$, as documented in Fig. 3.

Both exposure to hyperoxia and treatment with BAPN impacted collagen cross-linking in developing mouse lungs. Exposure of developing mouse lungs to 85% O$_2$ from the day of birth did not appreciably impact the noncollagen, nonelastin protein levels in the lungs (Table 2). However, exposure of developing mouse lungs to 85% O$_2$ from the day of birth increased collagen protein levels in the developing lungs. Increased collagen abundance was evident when collagen was assessed as total collagen per lung (63% increase; Fig. 4*A*) and

collagen content per total protein (42% increase; Fig. 4*B*). Additionally, exposure of developing mouse lungs to 85% O$_2$ from the day of birth increased collagen cross-linking, as assessed by the increased abundance of the (DHLNL) collagen cross-link (by 11%; Fig. 4*C*), although levels of the HP (Fig. 4*D*) and HLNL (Fig. 4*E*) cross-links were not impacted. However, the DHLNL-to-HLNL ratio (DHLNL/HLNL), which reflects the lysyl hydroxylation status in collagen cross-links (54) and is an index of the fibrotic status of tissue (63), was also increased (by 18%; Fig. 4*F*). Administration of BAPN to normally developing (exposed to 21% O$_2$) mice had no impact on collagen levels in the lung (Fig. 4, *A* and *B*); however, it did lead to decreased (by 31%; Fig. 4*D*) and increased (by 15%; Fig. 4*E*) HP and HLNL levels, respectively, in normally developing lungs. When administered concomitantly with hyperoxia exposure, BAPN reduced collagen abundance when collagen was assessed as total collagen per lung (24% decrease; Fig. 4*A*) and collagen content per total protein (12% decrease; Fig. 4*B*). Furthermore, BAPN reversed the impact of 85% O$_2$ exposure on the DHLNL/HLNL, which
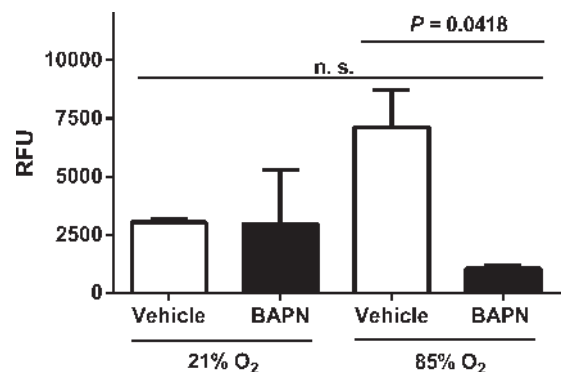

Fig. 3. Administration of BAPN normalized lung lysyl oxidase activity at a dose of 15 mg·kg^{-1}·day^{-1}. Lysyl oxidase activity was assessed using Amplex Red-based detection, in lung homogenates from solvent vehicle-treated and BAPN-treated mouse pups concomitantly exposed either to 21% O$_2$ or 85% O$_2$. Values are means ± SD. The *P* values were determined by one-way ANOVA with Tukey's post hoc test. RFU, relative fluorescence units; n.s., not significant ($P > 0.05$).

Table 2. *Effect of hyperoxia with or without BAPN administration on deposition of collagen in the developing mouse lung at postnatal day 19.5*

	21% O$_2$		85% O$_2$			
			Vehicle		BAPN	
Parameter	Vehicle (Mean ± SE)	BAPN (Mean ± SE)	Mean ± SE	P value vs. vehicle, 21% O$_2$	Mean ± SE	P value vs. vehicle, 85% O$_2$
NC-NE protein/lung, μg	2,387 ± 128.50	2,575 ± 81.40	2,784 ± 140.30	0.1763	2,440 ± 184.90	0.3143
Collagen/elastin, %	68.29 ± 5.19	64.60 ± 2.11	180.40 ± 12.18	<0.0001	144.00 ± 15.36	0.0723

Values are means ± SE; $n = 6$–7 lungs per group. Additional cross-link data are present in Fig. 4. BAPN, β-aminopropionitrile; NC-NE protein, noncollagen-nonelastin protein. P values were determined by one-way ANOVA with Tukey's post hoc analysis.

was normalized (was not significantly different from the 21% O$_2$-exposed, vehicle-treated mouse pups; Fig. 4*F*). A particularly striking effect of the exposure to 85% O$_2$ was a pronounced shift in the collagen-to-elastin ratio, which was threefold increased by 85% O$_2$ exposure (Table 2).

Both exposure to hyperoxia and treatment with BAPN impacted elastin cross-linking in developing mouse lungs. In stark contrast to the impact of inspired oxygen levels on collagen abundance in developing lungs, exposure of developing mouse lungs to 85% O$_2$ from the day of birth decreased insoluble elastin protein levels in the developing lungs [35% decrease assessed as total insoluble elastin percentage of total protein (Fig. 5*A*), or 38% decrease assessed as total insoluble elastin per lung (Table 3)]. Additionally, exposure of developing mouse lungs to 85% O$_2$ from the day of birth reduced the ratio of the desmosine to the isodesmosine elastin crosslinks
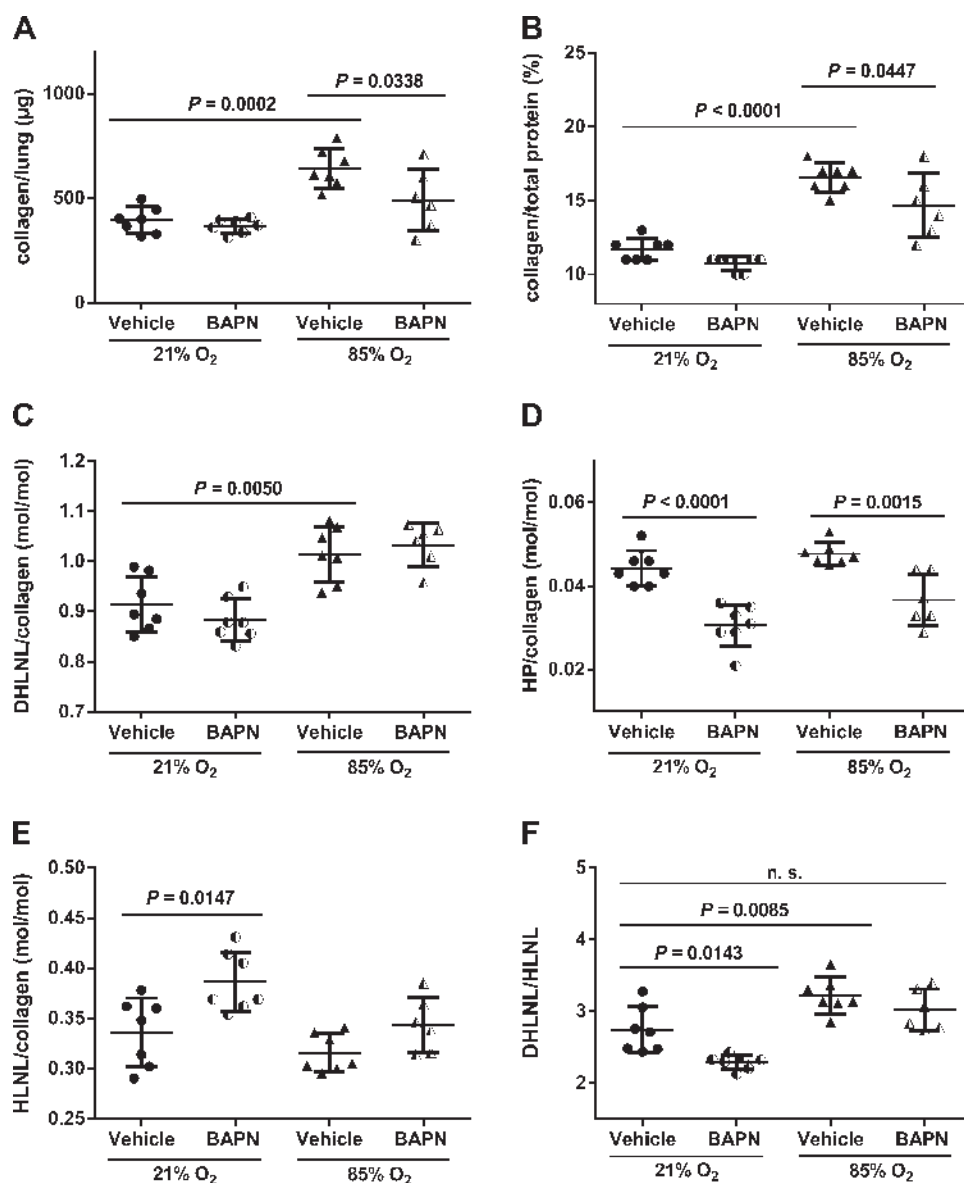

Fig. 4. Levels of total collagen and of collagen cross-links in the lungs of developing mouse pups were altered by hyperoxia exposure and BAPN administration. The abundance of collagen per lung (*A*), collagen per unit total protein (*B*), as well as the collagen cross-links dihydroxylysinonorleucine (DHLNL; *C*), hydroxylysylpyridinoline (HP; *D*), and hydroxylysinonorleucine (HLNL; *E*), were assessed in the lungs from solvent vehicle-treated and BAPN-treated mouse pups concomitantly exposed either to 21% O$_2$ or 85% O$_2$, at P19.5. *F*: additionally, the DHLNL-to-HLNL ratio is presented. Values are means ± SD ($n = 6$–7 per group). The P values were determined by one-way ANOVA with a Tukey's post hoc test. n.s., $P > 0.05$.

Fig. 5. Levels of total insoluble elastin and of cross-links in insoluble elastin in the lungs of developing mouse pups were altered by hyperoxia exposure and BAPN administration. The abundance of insoluble elastin per unit total protein (*A*), as well as the ratio of the elastin cross-links desmosine/isodesmosine (*B*), and the levels of desmosine (*C*), and isodesmosine (*D*) in insoluble elastin, were assessed in the lungs from solvent vehicle-treated and BAPN-treated mouse pups concomitantly exposed either to 21% O_2 or 85% O_2, at P19.5. Values are means ± SD (n = 6–7 per group). The P values were determined by one-way ANOVA with Tukey's post hoc test.
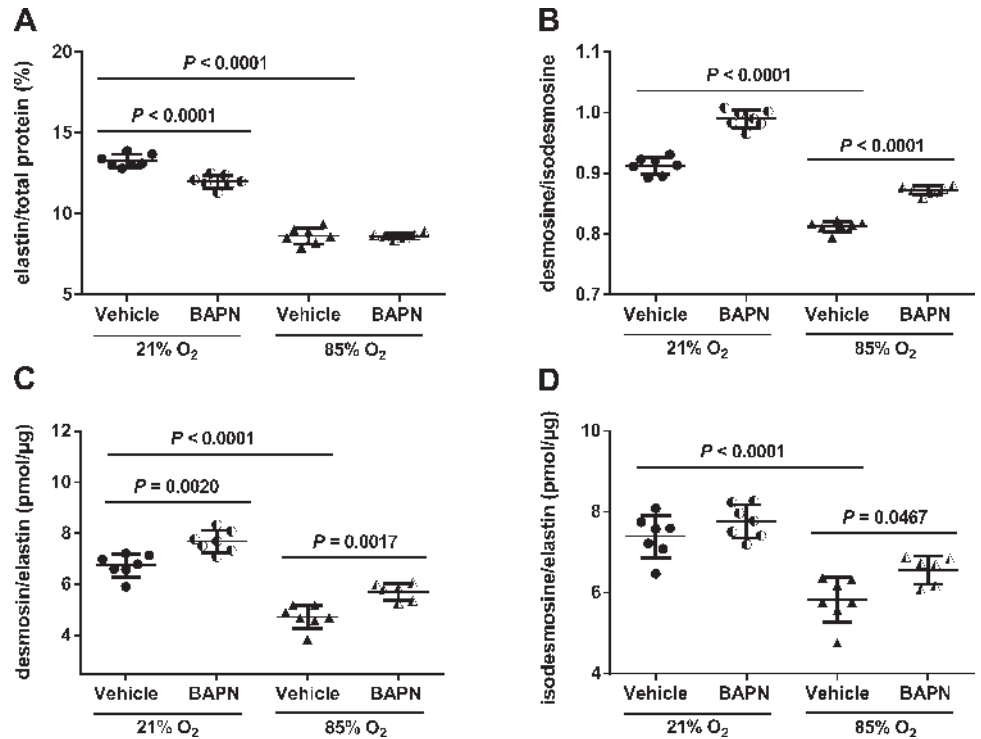
(by 11%; Fig. 5*B*). Furthermore, it decreased elastin cross-linking, as assessed by the decreased abundance of the desmosine elastin cross-link (by 30%; expressed as desmosine per unit insoluble elastin; Fig. 5*C*), and by the decreased abundance of the isodesmosine elastin cross-link (by 21%; expressed as isodesmosine per unit insoluble elastin; Fig. 5*D*). Administration of BAPN to normally developing (exposed to 21% O_2) mouse pups also reduced total insoluble elastin levels in the lung (by 10% Fig. 5*A*). Furthermore, BAPN administration to normally developing lungs increased the ratio of the desmosine to the isodesmosine elastin crosslinks (by 9%; Fig. 5*B*) and increased the abundance of desmosine (Fig. 5*C*) and isodesmosine (Fig. 5*D*) cross-links in insoluble elastin by 14 and 5%, respectively. When administered concomitantly with hyperoxia exposure, BAPN administration did not impact total elastin levels (Fig. 5*A*); however, BAPN administration did partially restore the desmosine-to-isodesmosine ratio (Fig. 5*B*) and partially restored desmosine (Fig. 5*C*) and isodesmosine (Fig. 5*D*) abundance in insoluble elastin.

Both exposure to hyperoxia and treatment with BAPN impacted elastin deposition in the parenchyma of developing mouse lungs. Elastin presents as focal structures ("dots") in the tips of developing septa in the immature lung (Fig. 6*A*).

Exposure of mouse pups to 85% O_2 from the day of birth resulted in an apparent arrest of alveolarization, evident by fewer and larger air spaces, at P9.5 (Fig. 6*B*). Exposure of developing mouse lungs to 85% O_2 from the day of birth reduced the apparent abundance of focal structures in the parenchyma of developing lungs at P9.5, where elastin fibers appeared more disorganized, by visual inspection. The administration of BAPN to normally developing (exposed to 21% O_2) mouse pups did not have any apparent impact on the elastin structures in the lung (Fig. 6*C*) at P9.5, compared with mouse pups that received solvent vehicle alone (Fig. 6*A*) at P9.5, by visual inspection. Lungs harvested at P19.5 revealed punctate elastin foci in the septa in the lungs of mice that were exposed to 21% O_2 from the day of birth, irrespective of whether solvent vehicle alone (Fig. 6*E*) or BAPN (Fig. 6*G*) was administered. Exposure of mouse pups to 85% O_2 from the day of birth resulted in a pronounced arrest of alveolarization, evident by fewer and larger air spaces, and also thickened septa at P19.5. These parameters are quantified in the next section. By visual inspection, the elastin fibers in the septa were largely devoid of punctate foci and were disorganized and "feathery" in appearance (Fig. 6*F*). Treatment of mouse pups from the day of birth with BAPN appeared to partially restore punctate

Table 3. *Effect of hyperoxia with or without BAPN administration on formation of elastin cross-links in developing mouse lung at postnatal day 19.5*

Parameter	21% O_2		85% O_2			
			Vehicle		BAPN	
	Vehicle (Mean ± SE)	BAPN (Mean ± SE)	Mean ± SE	P value vs. vehicle, 21% O_2	Mean ± SE	P value vs. vehicle, 85% O_2
Elastin/lung, μg	582.7 ± 16.00	569.1 ± 10.24	359.7 ± 14.75	<0.0001	350.9 ± 23.14	0.9815
(Des+Isodes)/elastin, pmol/μg	14.14 ± 0.364	15.45 ± 0.317	10.55 ± 0.383	<0.0001	12.28 ± 0.276	0.0098

Values are means ± SE; n = 6–7 lungs per group. Additional cross-link data are present in Fig. 5. Des, desmosine; Isodes, isodesmosine. P values were determined by one-way ANOVA with Tukey's post hoc analysis.
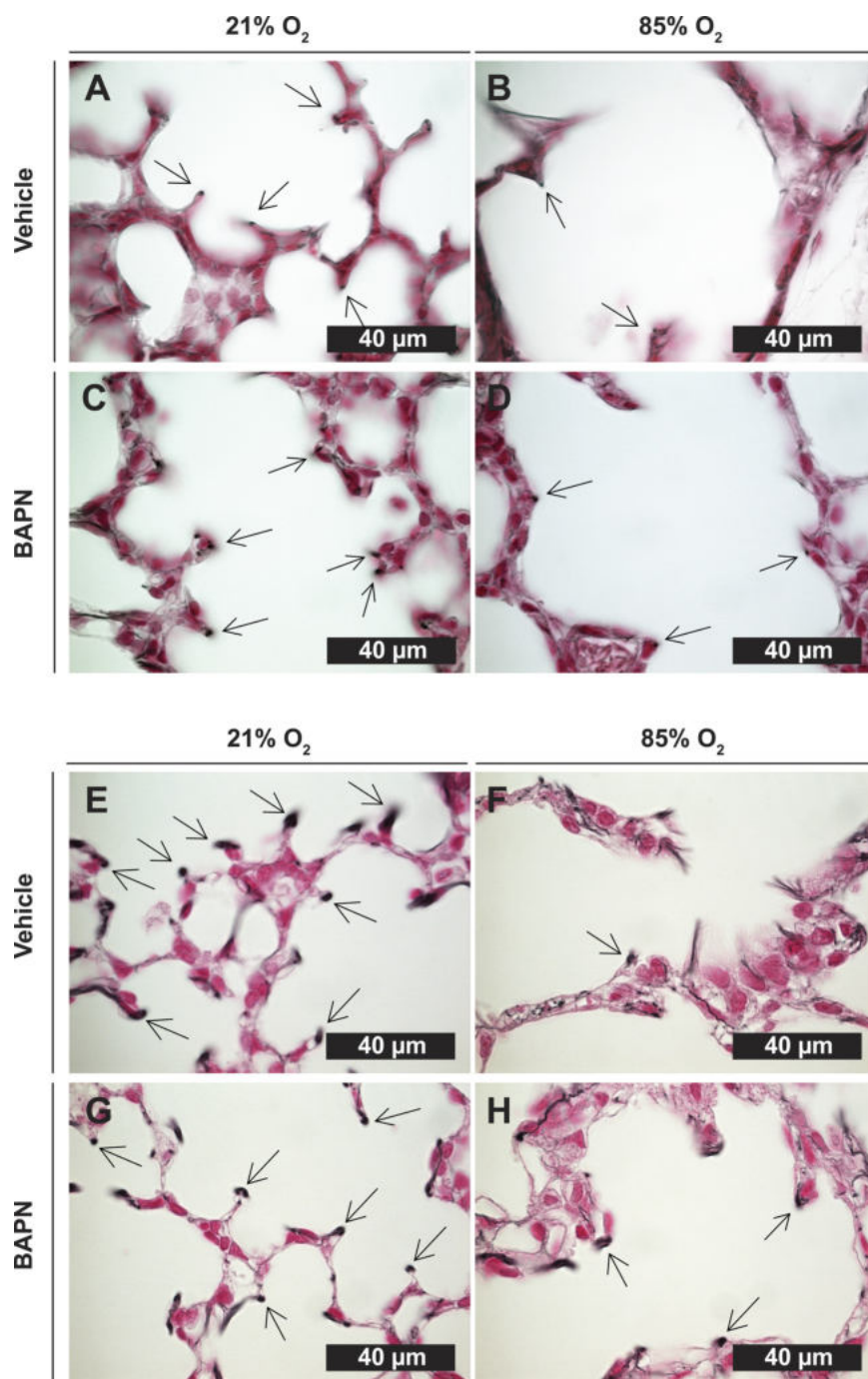
Fig. 6. Concomitant hyperoxia exposure and BAPN administration alters the appearance of elastin foci in the developing septa. Elastin was detected in paraffin-embedded lung tissue sections using Hart's elastic stain, in lungs from solvent vehicle-treated (*A*, *B*, *E*, *F*) and BAPN-treated (*C*, *D*, *G*, *H*) mouse pups concomitantly exposed either to 21% O_2 (*A*, *C*, *E*, *G*) or 85% O_2 (*B*, *D*, *F*, *H*), at P9.5 (*A–D*) and P19.5 (*E–H*). Arrows identify examples of elastin foci.

elastin foci to the septa (Fig. 6*H*), although septa remained clearly thickened and hypercellular, compared with septa in the 21% O_2-treated group.

Treatment of hyperoxia-exposed mouse pups with BAPN did not restore normal lung architecture. The changes in lung architecture seen by visual inspection of lung sections alluded to in the preceding paragraph were quantified by a designed-based stereomorphometric approach. The full spectrum of stereomorphometric data is provided for lungs from mice at P9.5 in Table 4, and for lungs from mice at P19.5 in Table 5. Key elements of the stereomorphometric analyses are provided for lungs from mice at P9.5 in Fig. 7, and for lungs from mice

at P19.5 in Fig. 8. In plastic-embedded lungs that were processed for stereomorphometric analysis by treatment with uranyl acetate and osmium tetroxide, visual inspection suggested that BAPN treatment generated a more complex lung than did solvent vehicle-treated lungs in pups exposed to 21% O_2 at P9.5 (Fig. 7, compare *A* and *C*). Exposure of mouse pups to 85% O_2 generated less complex lungs, with fewer, larger air spaces, evident by visual inspection (Fig. 7, compare *A* and *B*). Treatment of 85% O_2-exposed mouse pups with BAPN did not visibly impact lung complexity compared with lungs from solvent vehicle-treated mouse pups exposed to 85% O_2 (Fig. 7, compare *B* and *D*). Indeed, a stereological analysis revealed

Table 4. *Structural parameters of developing mouse lungs exposed to hyperoxia with or without BAPN administration at postnatal* day 9.5 *as assessed by stereological analysis*

| | 21% O_2 | | 85% O_2 | | | |
| | Vehicle (Mean ± SE) | BAPN (Mean ± SE) | Vehicle | | BAPN | |
Parameter			Mean ± SE	P value vs. vehicle, 21% O_2	Mean ± SE	P value vs. vehicle, 85% O_2
V (lung), cm^3	0.16 ± 0.011	0.18 ± 0.013	0.15 ± 0.006	0.9696	0.17 ± 0.011	0.4473
CV V (lung)	0.07	0.03		0.06		0.05
V_V (par/lung), %	88.81 ± 2.06	90.27 ± 1.11	88.19 ± 1.84	0.9936	87.13 ± 1.38	0.9688
V_V (nonpar/lung), %	11.19 ± 2,06	9.73 ± 1.11	11.81 ± 1.84	0.9936	12.87 ± 1.37	0.9688
N_V (alv/par) 10^7, cm^{-3}	1.25 ± 0.07	1.21 ± 0.07	0.84 ± 0.06	0.0021	0.94 ± 0.08	0.7935
S_V, cm^{-1}	651.46 ± 22.8	635.01 ± 14.68	438.51 ± 22.05	<0.0001	491.63 ± 23.47	0.0890
V_V (alv air/par), %	62.99 ± 2,67	61.39 ± 1.11	71.41 ± 1.60	0.0234	70.69 ± 1.73	0.9935
V (alv air, lung), cm^3	0.087 ± 0.006	0.098 ± 0.006	0.094 ± 0.005	0.7823	0.106 ± 0.006	0.4985
CV V (alv air, lung)	0.18	0.17		0.13		0.16
V (sep, lung), cm^3	0.051 ± 0.007	0.062 ± 0.005	0.013 ± 0.001	<0.0001	0.016 ± 0.002	0.9392
CV V (sep, lung)	0.38	0.22		0.23		0.33

Values are means ± SE; n = 7–8 lungs per group. V, volume; V_V, volume density; S_V, surface density; N_V, numerical density; CV, coefficient of variation; par, parenchyma; nonpar, nonparenchyma; sep, septa; alv air, alveolar air spaces; alv, alveoli. P values were determined by one-way ANOVA with Tukey's post hoc analysis.

that treatment of mouse pups from the day of birth with BAPN under 21% O_2 conditions did not appreciably alter lung structure, with the alveolar surface area [91.98 ± 27.77 cm^2 (solvent vehicle) vs. 101.40 ± 16.43 cm^2 (BAPN); Fig. 7*E*], septal thickness [11.02 ± 1.79 μm (solvent vehicle) vs. 12.06 ± 1.28 μm (BAPN); Fig. 7*F*], MLI [39.27 ± 7.51 μm (solvent vehicle) vs. 38.77 ± 2.70 μm (BAPN); Fig. 7*G*], and number of alveoli [1.75 ± 0.45 × 10^6 (solvent vehicle) vs. 1.96 ± 0.5402 × 10^6 (BAPN); Fig. 7*H*] unchanged at P9.5. Exposure of mouse pups from birth to 85% O_2 did dramatically impact alveolar surface area [91.98 ± 27.77 cm^2 (21% O_2) vs. 57.89 ± 7.26 cm^2 (85% O_2); Fig. 7*E*], MLI [39.27 ± 7.51 μm (21% O_2) vs. 65.39 ± 6.547 μm (85% O_2); Fig. 7*G*], and number of alveoli [1.746 ± 0.4495 × 10^6 (21% O_2) vs. 1.11 ± 0.27 × 10^6 (85% O_2); Fig. 7*H*] at P9.5. Treatment of 85% O_2-exposed mouse pups with BAPN did not appreciably alter any of these three parameters compared with solvent vehicle-treated pups exposed to 85% O_2 (Fig. 7, *E*, *G*, and *H*). There appeared to be a trend toward increased alveolar surface area (Fig. 7*E*), decreased septal thickness (Fig. 7*F*) and MLI (Fig. 7*G*), and increased alveoli number (Fig. 7*H*) when comparing the mean values of the solvent vehicle- vs. BAPN-treated

groups within the hyperoxia-exposed arm of the study; however, none of these changes was statistically significant. For this reason, it was speculated that a longer exposure time may highlight any corrective effects of BAPN administration to hyperoxia-exposed mouse pups. Therefore, the study was repeated for double the duration, and mouse lungs were harvested for stereomorphometric analysis at P19.5 (Fig. 8).

Visual inspection suggested that BAPN treatment did not generate a more complex lung than did solvent vehicle-treated lungs in pups exposed to 21% O_2 at P19.5 (Fig. 8, compare *A* and *C*). Exposure of mouse pups to 85% O_2 generated less complex lungs, with fewer, larger air spaces and thickened septa evident by visual inspection (Fig. 8, compare *A* and *B*). Treatment of 85% O_2-exposed mouse pups with BAPN did not visibly impact lung complexity compared with lungs from solvent vehicle-treated mouse pups exposed to 85% O_2 (Fig. 8, compared *B* and *D*). Furthermore, by visual inspection, within the 85% O_2-exposed group, BAPN treatment appeared to drive septal thickening (compare BAPN- and solvent vehicle-treated groups in Fig. 8*E*). Stereological analysis revealed that treatment of mouse pups from the day of birth with BAPN under 21% O_2 conditions did not appreciably impact alveolar surface

Table 5. *Structural parameters of developing mouse lungs exposed to hyperoxia with or without BAPN administration at postnatal* day 19.5 *as assessed by stereological analysis*

| | 21% O_2 | | 85% O_2 | | | |
| | Vehicle (mean ± SE) | BAPN (mean ± SE) | Vehicle | | BAPN | |
Parameter			Mean ± SE	P value vs. vehicle, 21% O_2	Mean ± SE	P value vs. vehicle, 85% O_2
V (lung), cm^3	0.26 ± 0.007	0.28 ± 0.011	0.27 ± 0.014	0.9669	0.26 ± 0.016	0.9851
CV V (lung)	0.07	0.09		0.12		0.14
V_V (par/lung), %	90.30 ± 0.969	90.22 ± 1.354	91.24 ± 0.922	0.9161	89.47 ± 0.767	0.6240
V_V (nonpar/lung), %	9.70 ± 0.969	9.78 ± 1.354	8.76 ± 0.922	0.9161	10.53 ± 0.767	0.6239
N_V (alv/par) 10^7, cm^{-3}	3.03 ± 0.21	3.44 ± 0.11	0.98 ± 0.10	<0.0001	1.11 ± 0.06	0.8811
S_V, cm^{-1}	877.20 ± 13.17	845.10 ± 17.15	476.40 ± 12.09	<0.0001	437.10 ± 17.85	0.3309
V_V (alv air/par), %	61.50 ± 0.55	61.70 ± 1.46	68.52 ± 1.28	0.0075	66.80 ± 1.65	0.7874
V (alv air, lung), cm^3	0.143 ± 0.004	0.157 ± 0.006	0.167 ± 0.013	0.3043	0.156 ± 0.012	0.8356
CV V (alv air, lung)	0.06	0.08		0.17		0.18
V (sep, lung), cm^3	0.090 ± 0.002	0.098 ± 0.005	0.076 ± 0.003	0.0543	0.076 ± 0.002	0.9993
CV V (sep, lung)	0.05	0.12		0.09		0.07

Values are means ± SE; n = 5 lungs per group. P values were determined by one-way ANOVA with Tukey's post hoc analysis.
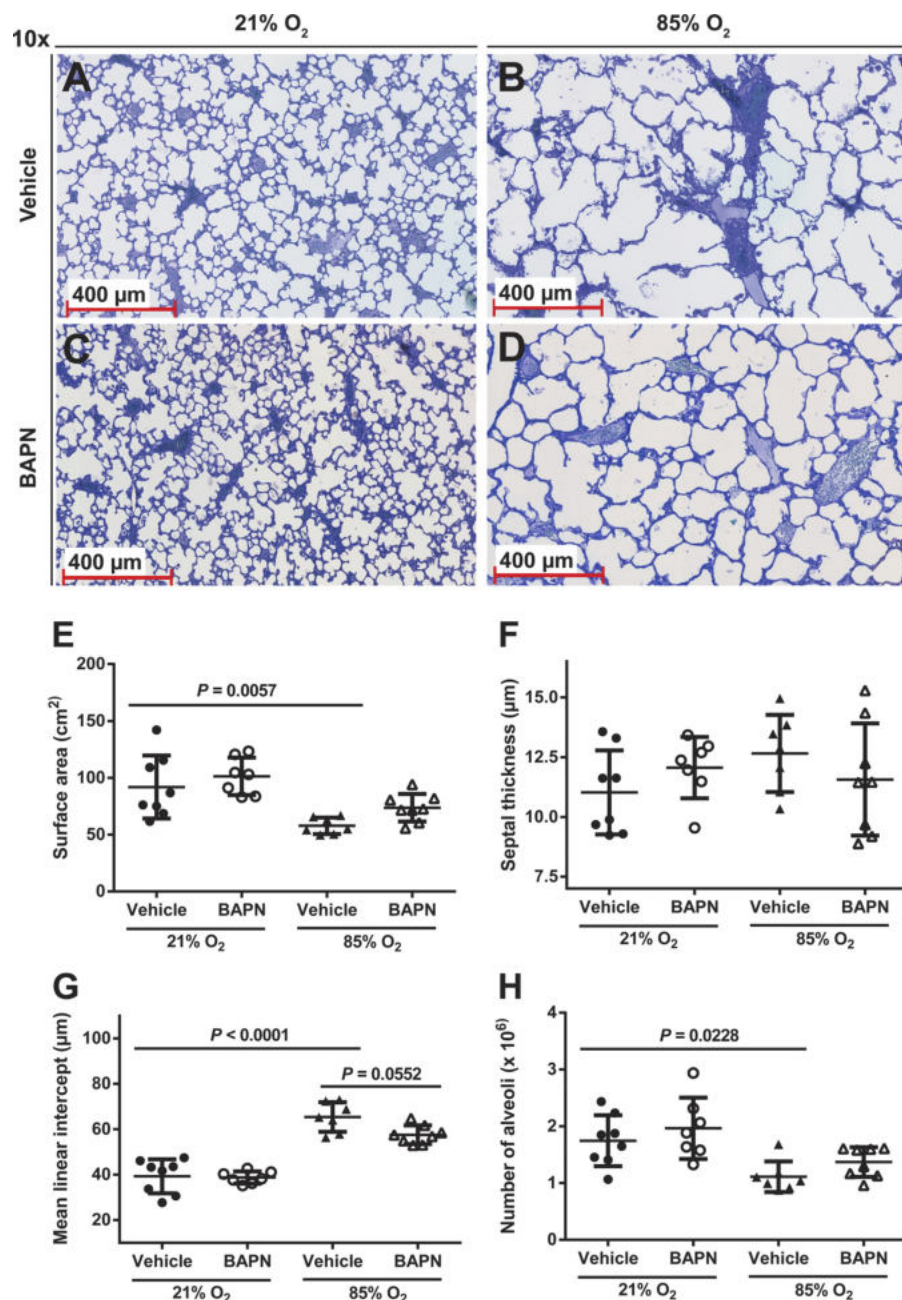
Fig. 7. Concomitant hyperoxia exposure and BAPN administration does not alter lung architecture in developing mouse pups at P9.5. Representative sections of plastic-embedded mouse lungs from solvent vehicle-treated (*A* and *B*) and BAPN-treated (*C* and *D*) mouse pups concomitantly exposed either to 21% O_2 (*A* and *C*) or 85% O_2 (*B* and *D*) at P9.5 are illustrated. Using a stereo-morphometric analysis, the alveolar surface area (*E*), septal thickness (*F*), mean linear intercept (*G*), and total number of alveoli in the lung (*H*) were determined. Values are means ± SD (*n* = 7–8 per group). The *P* values were determined by one-way ANOVA with Tukey's post hoc test. Additional stereo-morphometric parameters are provided in Table 4.

area [203.80 ± 11.71 cm^2 (solvent vehicle) vs. 215.4 ± 13.31 cm^2 (BAPN); Fig. 8*F*], septal thickness [8.80 ± 0.52 μm (solvent vehicle) vs. 9.082 ± 0.90 μm (BAPN); Fig. 8*G*], or MLI [28.06 ± 0.69 μm (solvent vehicle) vs. 29.25 ± 1.98 μm (BAPN); Fig. 8*H*] at P19.5. However, BAPN treatment of 21% O_2-exposed mouse pups did yield a moderate increase in the total number of alveoli [7.05 ± 1.10 × 10^6 (solvent vehicle) vs. 8.76 ± 0.33 × 10^6 (BAPN); Fig. 8*I*]. Exposure of mouse pups from birth to 85% O_2 did dramatically impact alveolar surface area [203.80 ± 11.71 cm^2 (21% O_2) vs. 115.00 ± 11.36 cm^2 (85% O_2); Fig. 8*F*], septal thickness [8.80 ± 0.52 μm (21% O_2) vs. 13.20 ± 0.96 μm (85% O_2); Fig. 8*G*], MLI [28.06 ± 0.69 μm (21% O_2) vs. 57.75 ± 5.22 μm (85% O_2); Fig. 8*H*], and number of alveoli [7.05 ± 1.10 × 10^6 (21% O_2) vs. 2.33 ± 0.43 × 10^6 (85% O_2); Fig. 8*I*] at P19.5. Treatment

of 85% O_2-exposed mouse pups with BAPN did not appreciably alter any of these parameters compared with solvent vehicle-treated pups exposed to 85% O_2, with the single exception of septal thickness, which was increased by BAPN treatment [13.20 ± 0.96 μm (solvent vehicle) vs. 15.18 ± 0.43 μm (BAPN); Fig. 8*G*], in line with the visibly increased septal thickness evident in Fig. 8*E*.

DISCUSSION

The aberrant late lung development associated with BPD is histopathologically characterized by a pronounced arrest of alveolarization, as a consequence of blunted secondary septation, leading to alveolar simplification, which is evident by a lower number of alveoli that are larger in size, in affected lungs
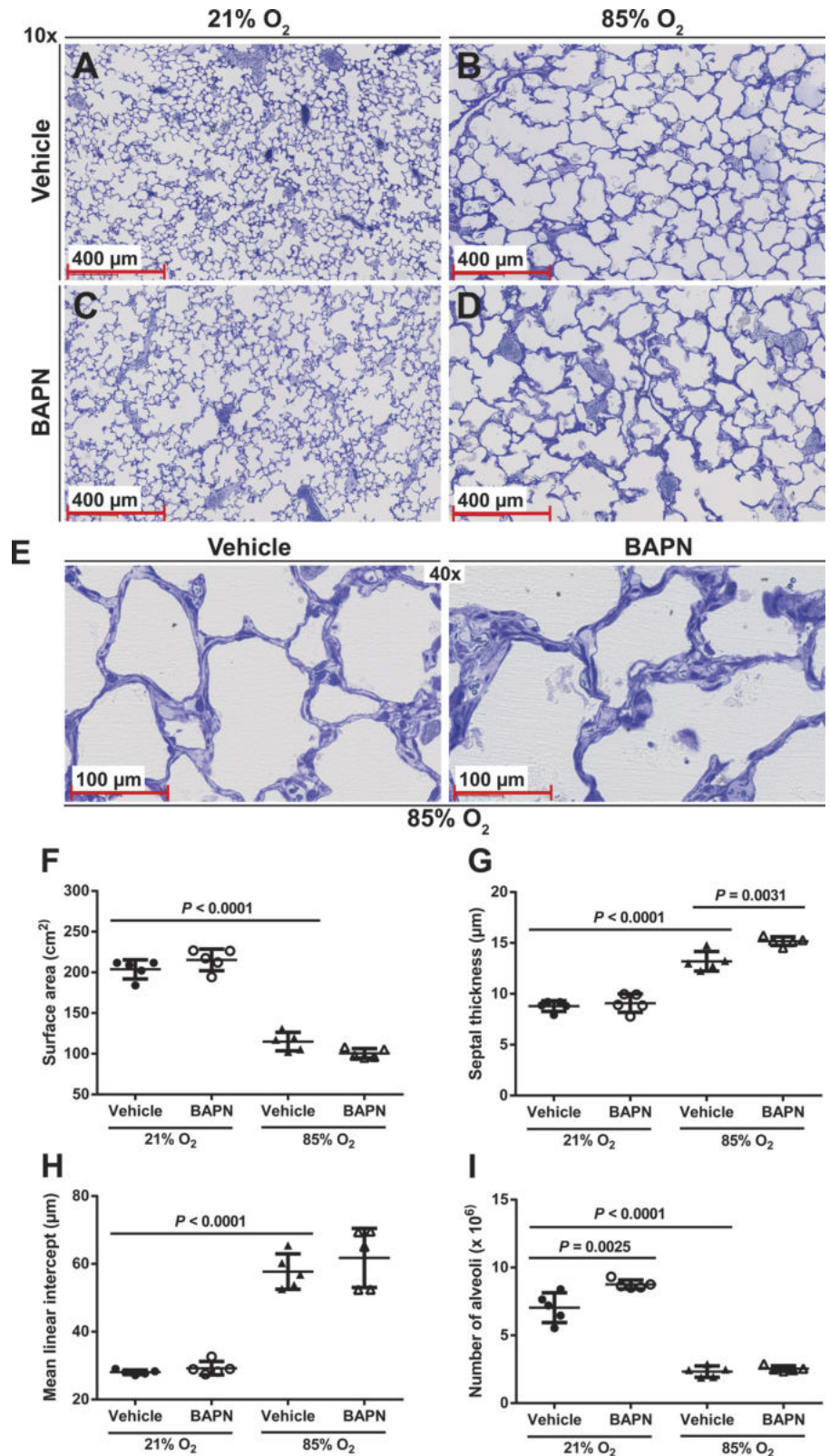
Fig. 8. Concomitant hyperoxia exposure and BAPN administration does alter lung architecture in developing mouse pups at P19.5. Representative sections of plastic-embedded mouse lungs from solvent vehicle-treated (*A* and *B*) and BAPN-treated (*C* and *D*) mouse pups concomitantly exposed either to 21% O$_2$ (*A* and *C*) or 85% O$_2$ (*B* and *D*) at P19.5 are illustrated. *E*: higher magnification images for the solvent vehicle-treated and BAPN-treated groups exposed to 85% O$_2$ are also provided. Using a stereo-morphometric analysis, the alveolar surface area (*F*), septal thickness (*G*), mean linear intercept (*H*), and total number of alveoli in the lung (*I*) were determined. Values are means ± SD (*n* = 5 per group). The *P* values were determined by one-way ANOVA with Tukey's post hoc test. Additional stereo-morphometric parameters are provided in Table 5.

(19, 27, 28). In addition to alveolar simplification, impacted lungs also exhibit pronounced perturbations to the ECM architecture, in particular, to the structure of collagen and elastin fibers in the parenchyma (59, 60). These changes, which include thickened and "twisted" parenchymal collagen fibers, as well as improperly deposited and remodeled elastin fibers, are observed in the lungs of human patients at risk for, or who have died with, BPD (11), as well as in the lungs of mice, rats,

baboons, and lambs, in which an arrest of alveolarization has been induced by exposure to elevated inspired oxygen concentrations, injurious mechanical ventilation, or combinations thereof (6, 13, 49, 66). Given the pivotal roles attributed to the ECM in directing both normal and aberrant late lung development, it has been speculated that these perturbations to ECM architecture may underlie the blunted secondary septation in affected lungs. However, to date, little is known about the molecular mechanisms that drive pathological changes to ECM architecture in impacted lungs: for example, what underlies the changes in abundance of ECM proteins, and why are collagen and elastin fibers malformed?

Recently, several studies have highlighted pathological changes in the expression and activity of several enzyme families in aberrantly developing lungs both in clinical BPD and in animal models of BPD. Among these enzyme families are the lysyl oxidases, lysyl hydroxylases, and transglutaminases, which drive the covalent intra- and intermolecular cross-linking of collagen and elastin fibers and, as such, modulate the posttranslational maturation of the ECM architecture of the lungs. Although increased pulmonary expression and activity of ECM cross-linking enzymes have been noted in clinical and experimental BPD, to date, *1*) no causal relationship has been established between elevated expression of ECM cross-linking enzymes and blunted alveolarization, and *2*) no study has demonstrated that ECM cross-linking is perturbed when alveolarization is blunted. Hence, in this study, selecting the lysyl oxidase family of ECM cross-linking enzymes, it was hypothesized that increased lysyl oxidase expression contributed to disturbed alveolarization in a hyperoxia-based mouse model of BPD, and the disturbed ECM cross-linking was associated with perturbed alveolarization in this model. To test this idea, the abundance of lysyl oxidase-generated cross-links in elastin and collagen was assessed in the lungs of mice in which alveolarization was arrested by exposure of developing mouse pups to elevated inspired oxygen concentrations, and lysyl oxidase activity was inhibited using broad-spectrum small-molecule inhibitor, to assess a causal role for lysyl oxidases in aberrant alveolarization that is characteristic of this animal model of BPD.

The lysyl oxidase family of copper-dependent amine oxidases comprises five members, named Lox and LoxL1 to LoxL4. The expression of lysyl oxidases is elevated in the lung in clinical BPD (33), in clinical and experimental pulmonary arterial hypertension (48), and in clinical and experimental lung fibrosis (16). In a mouse model of ventilator-induced disturbances to alveolarization in mice, changes in lysyl oxidase expression have also been noted (7, 9, 23). In the present study, in a hyperoxia-based mouse model of BPD, the abundance of multiple lysyl oxidases was elevated in the lungs of mice exposed to elevated inspired oxygen levels. Given that lysyl oxidase expression was hyperoxia responsive, lysyl oxidase activity was neutralized in vivo, in a well-characterized mouse model of BPD, using the pan-lysyl oxidase inhibitor BAPN. Daily administration of BAPN at a dose of 150 mg/kg dramatically reduced pup viability by P5.5, where mouse pups exhibited reduced milk intake, reduced body mass, and dramatically reduced mobility. This observation contrasts with observations made in adult mice, where BAPN was applied at the same dose and frequency to the same mouse strain in a rodent model of pulmonary arterial hypertension (48). In adult

mice, BAPN at a dose of 150 mg·kg^{-1}·day^{-1} was well tolerated, without any observable deleterious effects, and BAPN administration partially protected mice from hypoxia-driven increases in right ventricular systolic pressure. Additionally, BAPN administration helped preserve normal lung vascular matrix architecture, which is usually perturbed when pulmonary vessels are remodeled in response to hypoxia exposure (48). Thus these data underscore the importance of, and dangers of interfering with, ECM remodeling during organogenesis and development. These data are also in line with the reported perinatal lethality of mouse pups observed in $lox^{-/-}$ mice, which are thought to die from cardiorespiratory failure within 4 h of birth (24, 40). Similarly, while viable, $loxl1^{-/-}$ mice exhibit aortic aneurysms and diaphragmatic hernia, pointing to a role for a second member of the lysyl oxidase family in organogenesis and development (37). A lower BAPN dose, reduced by one log, to 15 mg·kg^{-1}·day^{-1}, was well tolerated by developing mouse pups, with no apparent deleterious effects on mouse viability. This BAPN dose was also sufficient to normalize lysyl oxidase activity in lung homogenates.

Mouse pups exposed to 85% O_2 from the day of birth demonstrated a pronounced increase in the levels of total insoluble collagen in the lung at P19.5. The increase in collagen levels may reflect either increased collagen transcription or decreased collagen turnover, in response to hyperoxia. Along these lines, it is interesting to note that lysyl oxidases, which may act as scaffolding proteins in transcription factor complexes (26, 55), have been reported to drive transcription of the $col3a1$ gene, encoding the collagen III α_1-subunit (18). As such, the elevated expression of lysyl oxidases may drive the elevated expression of collagens. However, other candidates also exist, such as transforming growth factor-β, since transforming growth factor-β signaling is both increased by exposure to hyperoxia and also drives collagen expression (3). Interestingly, concomitant treatment of hyperoxia-exposed mouse pups with BAPN dampened the ability of hyperoxia to drive increased collagen abundance in affected lungs. It may be speculated that *1*) the BAPN inhibited the protranscriptional activity of lysyl oxidases on, for example, the $col3a1$ promoter; or *2*) that decreased collagen cross-linking due to lysyl oxidase inhibition may have generated weakly cross-linked collagen peptides that were thus more amenable to proteolytic degradation, leading to less total collagen in the lungs of BAPN + hyperoxia-treated mice. At the same time, in contrast to the impact on collagen, exposure of newborn mouse pups to 85% O_2 depressed insoluble elastin levels in the lung. The collagen-to-elastin ratio of affected lungs was threefold increased, which would likely lead to a marked stiffening of the lung parenchyma. Given the importance of breathing motions and physical forces in driving alveolar development (41), the decreased lung compliance resulting from a shift in the collagen-to-elastin ratio almost certainly directly impacts the ability of the immature lung to develop properly (23).

Concerning the ECM cross-link status of mouse lungs following hyperoxia exposure, the abundance of the DHLNL collagen cross-link, as well as the DHLNL/HLNL, was increased in lungs from hyperoxia-exposed mice, suggestive of a profibrotic state (17, 63). The application of BAPN concomitantly with hyperoxia blunted this increase in lung collagen accumulation and partially normalized the DHLNL/HLNL. In summary, hyperoxia exposure drove alterations not only to

total insoluble collagen abundance in the lung, but also to collagen cross-linking in the lung, which could be partially reversed by BAPN administration, ostensibly by limiting the collagen cross-linking capacity of the increased lysyl oxidase activity observed in the lungs from hyperoxia-treated mice.

In contrast to collagen cross-links, hyperoxia exposure reduced the levels of the elastin cross-links desmosine and isodesmosine per unit lung elastin in the lung, and this trend was reversed with concomitant BAPN treatment. It appears counterintuitive that, in mice that were treated with BAPN, more desmosine and isodesmosine elastin cross-links were observed. Indeed, since these cross-links are generated by lysyl oxidase, one might expect to see less desmosine or isodesmosine in the lungs of BAPN-treated mice. It is not immediately apparent why this is the case, but several possible explanations may be offered. As mentioned above, the lysyl oxidases have attracted recent attention as scaffolding molecules in transcription factor complexes (18), where Lox, LoxL1, and LoxL2 may regulate gene transcription. It may be that among the spectrum of genes regulated by lysyl oxidases that are acting as transcription factors are genes encoding enzymes or chaperones that limit elastin cross-linking. Inhibition of lysyl oxidases with BAPN may thus be able to impact the formation of elastin cross-links separately from the direct cross-linking activity of lysyl oxidases, hence the paradoxical situation where inhibition of lysyl oxidases by BAPN under hyperoxic conditions actually increased the abundance of desmosine and isodesmosine in insoluble lung elastin. This idea is supported by the observation that, under normoxic conditions, BAPN administration also drive increased desmosine abundance (compare the vehicle and BAPN groups under 21% O_2 in Fig. 5C). Clearly, a lysyl oxidase-independent role for BAPN in the positive regulation of elastin cross-linking has not been ruled out. Alternatively, the dramatically shifted ratio of collagen to elastin may play a role in regulating lysyl oxidase activity on elastin. Lysyl oxidases physically associate with collagen fibers and other ECM structures, and the vastly increased abundance of collagen may have sequestered lysyl oxidases, making these enzymes less available to elastin, hence the reduced abundance of elastin cross-links in the hyperoxia groups. The latter idea gains credence from the observation in Fig. 4A (vehicle vs. BAPN groups within the 85% O_2 arm), where BAPN administration under hyperoxic conditions reduced total lung collagen, which was associated with increased elastin cross-linking (Fig. 5, C and D; vehicle vs. BAPN groups within the 85% O_2 arm), perhaps due to less lysyl oxidase sequestering by less total collagen. Irrespectively, an examination of the form and abundance of elastin foci in the developing lungs suggested that BAPN treatment under hyperoxic conditions generated more elastic foci in developing septa ("dots" indicated by arrows in Fig. 6, H vs. F) than were apparently present in vehicle-treated lungs under hyperoxic conditions.

Since BAPN administration under hyperoxic conditions partially normalized total lung collagen, the abundance of selected collagen and elastin cross-links, and elastin foci distribution in the developing septa, it was postulated that BAPN administration may improve lung architecture in mice exposed to hyperoxia during the neonatal period. Indeed, in mice exposed to hyperoxia for 9 days that concomitantly received BAPN, the mean values for surface area, septal thickness, MLI, and total number of alveoli in the lung all trended in an "improved" direction (i.e., toward the vehicle/21% O_2 values), from the 85% O_2/vehicle values, although no difference achieved a P value <0.05. For this reason, the study was extended for an additional 10 days. However, an additional 10 days of BAPN administration concomitant with hyperoxia exposure did not appreciably improve lung architecture compared with vehicle-treated, hyperoxia-exposed lungs, where the mean values for surface area, MLI, and total number of alveoli in the lung were unchanged between the 85% O_2/BAPN and 85% O_2/vehicle groups, and the septal thickness was markedly increased in the 85% O_2/BAPN group compared with the 85% O_2/vehicle group. This is not the first report on the effects of BAPN administration on late lung development. Indeed, Kida and Thurlbeck (29, 30) described the impact of BAPN administration on normal late lung development in healthy rat pups in 1980, where very high doses of BAPN were deleterious and impeded normal alveolarization. This is consistent with reports that targeted deletion of lysyl oxidases impacts the development of the cardiorespiratory system (24, 37, 40).

In interpreting these data, it is clearly important to remember that there is no good animal model of clinical BPD that recapitulates all pathological aspects of clinical BPD. The hyperoxia model largely recapitulates the blunted secondary septation seen in BPD. However, hyperoxia is a different injurious stimulus than is, for example, the inflammation seen in chorioamnionitis (32). Indeed, the role of antenatal inflammation (34) and the interaction of steroid signaling and inflammatory pathways (15, 35) have been demonstrated to modulate key pathogenic signaling pathways in a sheep model of BPD. This represents a key limitation of the hyperoxia model, and how lysyl oxidases impact ECM remodeling in other animal models of BPD has not been addressed in this study. Our study has also not addressed how vitamin A or steroids may alter ECM maturation, which is most likely a relevant line of investigation, given that both vitamin A (1) and steroids (53) are reported to modulate the formation of ECM structures in BPD animal models.

Thus, in summary, the exposure of immature mouse lungs to normobaric hyperoxia perturbed lung architecture increased the abundance of collagen and collagen cross-links and decreased the abundance of elastin and elastin cross-links. These perturbations to ECM cross-linking may underlie some of the aberrant ECM structures observed in affected lungs. These changes were also accompanied by increased expression of lysyl oxidases in the lung. However, antagonizing lysyl oxidase activity with the pan-lysyl oxidase inhibitor BAPN did not lead to any improvement in lung architecture, despite partially normalizing total collagen abundance, the abundance of some collagen and elastin cross-links, and elastin foci distribution in developing septa. These data highlight a possible role for perturbed ECM structures as an underlying cause of blunted alveolarization in response to hyperoxia exposure; however, these data do not support the antagonism of lysyl oxidases as an avenue to drive the normalization of alveolar development in oxygen-injured developing lungs.

Pierce (Barnes-Jewish Hospital, Washington University School of Medicine, St. Louis, MO), Stephen E. McGowan (Department of Internal Medicine, Carver College of Medicine, University of Iowa, Iowa City, IA), and Thomas J. Mariani (School of Medicine and Dentistry, University of Rochester Medical Center, Rochester, NY) for valuable advice.

DISCLOSURES

No conflicts of interest, financial or otherwise are declared by the author(s).

AUTHOR CONTRIBUTIONS

Author contributions: I.M. and R.E.M. conception and design of research; I.M., J.R.-C., H.S., A.M., and J.B. performed experiments; I.M., H.S., I.V., S.H., K.M., W.S., J.B., and R.E.M. analyzed data; I.M., W.S., and R.E.M. interpreted results of experiments; I.M. prepared figures; I.M., W.S., and R.E.M. drafted manuscript; I.M., J.R.-C., H.S., A.M., I.V., S.H., K.M., W.S., J.B., and R.E.M. edited and revised manuscript; I.M., J.R.-C., H.S., A.M., I.V., S.H., K.M., W.S., J.B., and R.E.M. approved final version of manuscript.

REFERENCES

1. **Albertine KH, Dahl MJ, Gonzales LW, Wang ZM, Metcalfe D, Hyde DM, Plopper CG, Starcher BC, Carlton DP, Bland RD.** Chronic lung disease in preterm lambs: effect of daily vitamin A treatment on alveolarization. *Am J Physiol Lung Cell Mol Physiol* 299: L59–L72, 2010.
2. **Albertine KH, Jones GP, Starcher BC, Bohnsack JF, Davis PL, Cho SC, Carlton DP, Bland RD.** Chronic lung injury in preterm lambs. Disordered respiratory tract development. *Am J Respir Crit Care Med* 159: 945–958, 1999.
3. **Alejandre-Alcázar MA, Kwapiszewska G, Reiss I, Amarie OV, Marsh LM, Sevilla-Perez J, Wygrecka M, Eul B, Köbrich S, Hesse M, Schermuly RT, Seeger W, Eickelberg O, Morty RE.** Hyperoxia modulates TGF-beta/BMP signaling in a mouse model of bronchopulmonary dysplasia. *Am J Physiol Lung Cell Mol Physiol* 292: L537–L549, 2007.
4. **Alejandre-Alcázar MA, Michiels-Corsten M, Vicencio AG, Reiss I, Ryu J, de Krijger RR, Haddad GG, Tibboel D, Seeger W, Eickelberg O, Morty RE.** TGF-beta signaling is dynamically regulated during the alveolarization of rodent and human lungs. *Dev Dyn* 237: 259–269, 2008.
5. **Alejandre-Alcázar MA, Shalamanov PD, Amarie OV, Sevilla-Pérez J, Seeger W, Eickelberg O, Morty RE.** Temporal and spatial regulation of bone morphogenetic protein signaling in late lung development. *Dev Dyn* 236: 2825–2835, 2007.
6. **Berger J, Bhandari V.** Animal models of bronchopulmonary dysplasia. The term mouse models. *Am J Physiol Lung Cell Mol Physiol* 307: L936–L947, 2014.
7. **Bland RD, Ertsey R, Mokres LM, Xu L, Jacobson BE, Jiang S, Alvira CM, Rabinovitch M, Shinwell ES, Dixit A.** Mechanical ventilation uncouples synthesis and assembly of elastin and increases apoptosis in lungs of newborn mice. Prelude to defective alveolar septation during lung development? *Am J Physiol Lung Cell Mol Physiol* 294: L3–L14, 2008.
8. **Bland RD, Mokres LM, Ertsey R, Jacobson BE, Jiang S, Rabinovitch M, Xu L, Shinwell ES, Zhang F, Beasley MA.** Mechanical ventilation with 40% oxygen reduces pulmonary expression of genes that regulate lung development and impairs alveolar septation in newborn mice. *Am J Physiol Lung Cell Mol Physiol* 293: L1099–L1110, 2007.
9. **Bland RD, Xu L, Ertsey R, Rabinovitch M, Albertine KH, Wynn KA, Kumar VH, Ryan RM, Swartz DD, Csiszar K, Fong KS.** Dysregulation of pulmonary elastin synthesis and assembly in preterm lambs with chronic lung disease. *Am J Physiol Lung Cell Mol Physiol* 292: L1370–L1384, 2007.
10. **Brinckmann J, Kim S, Wu J, Reinhardt DP, Batmunkh C, Metzen E, Notbohm H, Bank RA, Krieg T, Hunzelmann N.** Interleukin 4 and prolonged hypoxia induce a higher gene expression of lysyl hydroxylase 2 and an altered cross-link pattern: important pathogenetic steps in early and late stage of systemic scleroderma? *Matrix Biol* 24: 459–468, 2005.
11. **Bruce MC, Pawlowski R, Tomashefski JF Jr.** Changes in lung elastic fiber structure and concentration associated with hyperoxic exposure in the developing rat lung. *Am Rev Respir Dis* 140: 1067–1074, 1989.
12. **Bruce MC, Wedig KE, Jentoft N, Martin RJ, Cheng PW, Boat TF, Fanaroff AA.** Altered urinary excretion of elastin cross-links in premature infants who develop bronchopulmonary dysplasia. *Am Rev Respir Dis* 131: 568–572, 1985.
13. **Buczynski BW, Maduekwe ET, O'Reilly MA.** The role of hyperoxia in the pathogenesis of experimental BPD. *Semin Perinatol* 37: 69–78, 2013.
14. **Cherukupalli K, Larson JE, Rotschild A, Thurlbeck WM.** Biochemical, clinical, and morphologic studies on lungs of infants with bronchopulmonary dysplasia. *Pediatr Pulmonol* 22: 215–229, 1996.
15. **Collins JJ, Kunzmann S, Kuypers E, Kemp MW, Speer CP, Newnham JP, Kallapur SG, Jobe AH, Kramer BW.** Antenatal glucocorticoids counteract LPS changes in TGF-beta pathway and caveolin-1 in ovine fetal lung. *Am J Physiol Lung Cell Mol Physiol* 304: L438–L444, 2013.
16. **Counts DF, Evans JN, Dipetrillo TA, Sterling KM Jr, Kelley J.** Collagen lysyl oxidase activity in the lung increases during bleomycin-induced lung fibrosis. *J Pharmacol Exp Ther* 219: 675–678, 1981.
17. **Gerriets JE, Reiser KM, Last JA.** Lung collagen cross-links in rats with experimentally induced pulmonary fibrosis. *Biochim Biophys Acta* 1316: 121–131, 1996.
18. **Giampuzzi M, Botti G, Di Duca M, Arata L, Ghiggeri G, Gusmano R, Ravazzolo R, Di Donato A.** Lysyl oxidase activates the transcription activity of human collagene III promoter. Possible involvement of Ku antigen. *J Biol Chem* 275: 36341–36349, 2000.
19. **Hadchouel A, Franco-Montoya ML, Delacourt C.** Altered lung development in bronchopulmonary dysplasia. *Birth Defects Res A Clin Mol Teratol* 100: 158–167, 2014.
20. **Herriges M, Morrisey EE.** Lung development: orchestrating the generation and regeneration of a complex organ. *Development* 141: 502–513, 2014.
21. **Hilgendorff A, Parai K, Ertsey R, Jain N, Navarro EF, Peterson JL, Tamosiuniene R, Nicolls MR, Starcher BC, Rabinovitch M, Bland RD.** Inhibiting lung elastase activity enables lung growth in mechanically ventilated newborn mice. *Am J Respir Crit Care Med* 184: 537–546, 2011.
22. **Hilgendorff A, Parai K, Ertsey R, Juliana Rey-Parra G, Thebaud B, Tamosiuniene R, Jain N, Navarro EF, Starcher BC, Nicolls MR, Rabinovitch M, Bland RD.** Neonatal mice genetically modified to express the elastase inhibitor elafin are protected against the adverse effects of mechanical ventilation on lung growth. *Am J Physiol Lung Cell Mol Physiol* 303: L215–L227, 2012.
23. **Hilgendorff A, Parai K, Ertsey R, Navarro EF, Jain N, Carandang F, Peterson J, Mokres LM, Milla C, Preuss S, Alejandre Alcazar MA, Khan S, Masumi J, Ferreira-Tojais N, Mujahid S, Starcher BC, Rabinovitch M, Bland RD.** Lung matrix and vascular remodeling in mechanically ventilated elastin haplo-insufficient (Eln+/−) newborn mice. *Am J Physiol Lung Cell Mol Physiol* 308: L464–L478, 2015.
24. **Hornstra IK, Birge S, Starcher B, Bailey AJ, Mecham RP, Shapiro SD.** Lysyl oxidase is required for vascular and diaphragmatic development in mice. *J Biol Chem* 278: 14387–14393, 2003.
25. **Hsia CC, Hyde DM, Ochs M, Weibel ER.** An official research policy statement of the American Thoracic Society/European Respiratory Society: standards for quantitative assessment of lung structure. *Am J Respir Crit Care Med* 181: 394–418, 2010.
26. **Iturbide A, Garcia de Herreros A, Peiro S.** A new role for LOX and LOXL2 proteins in transcription regulation. *FEBS J.* In press.
27. **Jain D, Bancalari E.** Bronchopulmonary dysplasia: clinical perspective. *Birth Defects Res A Clin Mol Teratol* 100: 134–144, 2014.
28. **Jobe AH.** What is BPD in 2012 and what will BPD become? *Early Hum Dev* 88, *Suppl* 2: S27–S28, 2012.
29. **Kida K, Thurlbeck WM.** The effects of beta-aminopropionitrile on the growing rat lung. *Am J Pathol* 101: 693–710, 1980.
30. **Kida K, Thurlbeck WM.** Lack of recovery of lung structure and function after the administration of beta-amino-propionitrile in the postnatal period. *Am Rev Respir Dis* 122: 467–475, 1980.
31. **Knudsen L, Ochs M, Mackay R, Townsend P, Deb R, Muhlfeld C, Richter J, Gilbert F, Hawgood S, Reid K, Clark H.** Truncated recombinant human SP-D attenuates emphysema and type II cell changes in SP-D deficient mice. *Respir Res* 8: 70, 2007.

32. **Kramer BW.** Chorioamnionitis–new ideas from experimental models. *Neonatology* 99: 320–325, 2011.

33. **Kumarasamy A, Schmitt I, Nave AH, Reiss I, van der Horst I, Dony E, Roberts JD Jr, de Krijger RR, Tibboel D, Seeger W, Schermuly RT, Eickelberg O, Morty RE.** Lysyl oxidase activity is dysregulated during impaired alveolarization of mouse and human lungs. *Am J Respir Crit Care Med* 180: 1239–1252, 2009.

34. **Kunzmann S, Speer CP, Jobe AH, Kramer BW.** Antenatal inflammation induced TGF-beta1 but suppressed CTGF in preterm lungs. *Am J Physiol Lung Cell Mol Physiol* 292: L223–L231, 2007.

35. **Kuypers E, Collins JJ, Kramer BW, Ofman G, Nitsos I, Pillow JJ, Polglase GR, Kemp MW, Newnham JP, Gavilanes AW, Nowacki R, Ikegami M, Jobe AH, Kallapur SG.** Intra-amniotic LPS and antenatal betamethasone: inflammation and maturation in preterm lamb lungs. *Am J Physiol Lung Cell Mol Physiol* 302: L380–L389, 2012.

36. **Liu S, Young SM, Varisco BM.** Dynamic expression of chymotrypsin-like elastase 1 over the course of murine lung development. *Am J Physiol Lung Cell Mol Physiol* 306: L1104–L1116, 2014.

37. **Liu X, Zhao Y, Gao J, Pawlyk B, Starcher B, Spencer JA, Yanagisawa H, Zuo J, Li T.** Elastic fiber homeostasis requires lysyl oxidase-like 1 protein. *Nat Genet* 36: 178–182, 2004.

38. **Madurga A, Mižíková I, Ruiz-Camp J, Morty RE.** Recent advances in late lung development and the pathogenesis of bronchopulmonary dysplasia. *Am J Physiol Lung Cell Mol Physiol* 305: L893–L905, 2013.

39. **Madurga A, Mižíková I, Ruiz-Camp J, Vadász I, Herold S, Mayer K, Fehrenbach H, Seeger W, Morty RE.** Systemic hydrogen sulfide administration partially restores normal alveolarization in an experimental animal model of bronchopulmonary dysplasia. *Am J Physiol Lung Cell Mol Physiol* 306: L684–L697, 2014.

40. **Mäki JM, Sormunen R, Lippo S, Kaarteenaho-Wiik R, Soininen R, Myllyharju J.** Lysyl oxidase is essential for normal development and function of the respiratory system and for the integrity of elastic and collagen fibers in various tissues. *Am J Pathol* 167: 927–936, 2005.

41. **Mammoto T, Jiang E, Jiang A, Mammoto A.** Extracellular matrix structure and tissue stiffness control postnatal lung development through the lipoprotein receptor-related protein 5/Tie2 signaling system. *Am J Respir Cell Mol Biol* 49: 1009–1018, 2013.

42. **Mariani TJ, Reed JJ, Shapiro SD.** Expression profiling of the developing mouse lung: insights into the establishment of the extracellular matrix. *Am J Respir Cell Mol Biol* 26: 541–548, 2002.

43. **Mariani TJ, Sandefur S, Pierce RA.** Elastin in lung development. *Exp Lung Res* 23: 131–145, 1997.

44. **Moore AM, Buch S, Han RN, Freeman BA, Post M, Tanswell AK.** Altered expression of type I collagen, TGF-beta 1, and related genes in rat lung exposed to 85% O2. *Am J Physiol Lung Cell Mol Physiol* 268: L78–L84, 1995.

45. **Morrisey EE, Cardoso WV, Lane RH, Rabinovitch M, Abman SH, Ai X, Albertine KH, Bland RD, Chapman HA, Checkley W, Epstein JA, Kintner CR, Kumar M, Minoo P, Mariani TJ, McDonald DM, Mukouyama YS, Prince LS, Reese J, Rossant J, Shi W, Sun X, Werb Z, Whitsett JA, Gail D, Blaisdell CJ, Lin QS.** Molecular determinants of lung development. *Ann Am Thorac Soc* 10: S12–S16, 2013.

46. **Morty RE, Nejman B, Kwapiszewska G, Hecker M, Zakrzewicz A, Kouri FM, Peters DM, Dumitrascu R, Seeger W, Knaus P, Schermuly RT, Eickelberg O.** Dysregulated bone morphogenetic protein signaling in monocrotaline-induced pulmonary arterial hypertension. *Arterioscler Thromb Vasc Biol* 27: 1072–1078, 2007.

47. **Mühlfeld C, Ochs M.** Quantitative microscopy of the lung: a problem-based approach. Part 2: Stereological parameters and study designs in various diseases of the respiratory tract. *Am J Physiol Lung Cell Mol Physiol* 305: L205–L221, 2013.

48. **Nave AH, Mižíková I, Niess G, Steenbock H, Reichenberger F, Talavera ML, Veit F, Herold S, Mayer K, Vadász I, Weissmann N, Seeger W, Brinckmann J, Morty RE.** Lysyl oxidases play a causal role in vascular remodeling in clinical and experimental pulmonary arterial hypertension. *Arterioscler Thromb Vasc Biol* 34: 1446–1458, 2014.

49. **O'Reilly M, Thebaud B.** Animal models of bronchopulmonary dysplasia. The term rat models. *Am J Physiol Lung Cell Mol Physiol* 307: L948–L958, 2014.

50. **Ochs M.** A brief update on lung stereology. *J Microsc* 222: 188–200, 2006.

51. **Ochs M, Mühlfeld C.** Quantitative microscopy of the lung: a problem-based approach. Part 1: Basic principles of lung stereology. *Am J Physiol Lung Cell Mol Physiol* 305: L15–L22, 2013.

52. **Pierce RA, Albertine KH, Starcher BC, Bohnsack JF, Carlton DP, Bland RD.** Chronic lung injury in preterm lambs: disordered pulmonary elastin deposition. *Am J Physiol Lung Cell Mol Physiol* 272: L452–L460, 1997.

53. **Pierce RA, Mariencheck WI, Sandefur S, Crouch EC, Parks WC.** Glucocorticoids upregulate tropoelastin expression during late stages of fetal lung development. *Am J Physiol Lung Cell Mol Physiol* 268: L491–L500, 1995.

54. **Pornprasertsuk S, Duarte WR, Mochida Y, Yamauchi M.** Lysyl hydroxylase-2b directs collagen cross-linking pathways in MC3T3-E1 cells. *J Bone Miner Res* 19: 1349–1355, 2004.

55. **Rodriguez C, Martinez-Gonzalez J, Raposo B, Alcudia JF, Guadall A, Badimon L.** Regulation of lysyl oxidase in vascular cells: lysyl oxidase as a new player in cardiovascular diseases. *Cardiovasc Res* 79: 7–13, 2008.

56. **Schneider JP, Ochs M.** Alterations of mouse lung tissue dimensions during processing for morphometry: a comparison of methods. *Am J Physiol Lung Cell Mol Physiol* 306: L341–L350, 2014.

57. **Shifren A, Durmowicz AG, Knutsen RH, Hirano E, Mecham RP.** Elastin protein levels are a vital modifier affecting normal lung development and susceptibility to emphysema. *Am J Physiol Lung Cell Mol Physiol* 292: L778–L787, 2007.

58. **Swee MH, Parks WC, Pierce RA.** Developmental regulation of elastin production. Expression of tropoelastin pre-mRNA persists after down-regulation of steady-state mRNA levels. *J Biol Chem* 270: 14899–14906, 1995.

59. **Thibeault DW, Mabry SM, Ekekezie II, Truog WE.** Lung elastic tissue maturation and perturbations during the evolution of chronic lung disease. *Pediatrics* 106: 1452–1459, 2000.

60. **Thibeault DW, Mabry SM, Ekekezie II, Zhang X, Truog WE.** Collagen scaffolding during development and its deformation with chronic lung disease. *Pediatrics* 111: 766–776, 2003.

61. **Tschanz SA, Burri PH, Weibel ER.** A simple tool for stereological assessment of digital images: the STEPanizer. *J Microsc* 243: 47–59, 2011.

62. **Weibel ER, Hsia CC, Ochs M.** How much is there really? Why stereology is essential in lung morphometry. *J Appl Physiol (1985)* 102: 459–467, 2007.

63. **Willenborg S, Eckes B, Brinckmann J, Krieg T, Waisman A, Hartmann K, Roers A, Eming SA.** Genetic ablation of mast cells redefines the role of mast cells in skin wound healing and bleomycin-induced fibrosis. *J Invest Dermatol* 134: 2005–2015, 2014.

64. **Witsch TJ, Niess G, Sakkas E, Likhoshvay T, Becker S, Herold S, Mayer K, Vadász I, Roberts JD Jr, Seeger W, Morty RE.** Transglutaminase 2: a new player in bronchopulmonary dysplasia? *Eur Respir J* 44: 109–121, 2014.

65. **Witsch TJ, Turowski P, Sakkas E, Niess G, Becker S, Herold S, Mayer K, Vadász I, Roberts JD Jr, Seeger W, Morty RE.** Deregulation of the lysyl hydroxylase matrix cross-linking system in experimental and clinical bronchopulmonary dysplasia. *Am J Physiol Lung Cell Mol Physiol* 306: L246–L259, 2014.

66. **Yoder BA, Coalson JJ.** Animal models of bronchopulmonary dysplasia. The preterm baboon models. *Am J Physiol Lung Cell Mol Physiol* 307: L970–L977, 2014.